# Analysis for optical transmission characteristic of $Fe_3O_4$ @ $TiO_2$ core @ shell colloidal photonic crystals

HUANG Yan， LIANG Gong-Ying， HUO Ge， LU Xue-Gang*

（School of Science，Key Laboratory of Shanxi for Advanced Materials and Mesoscopic Physics，State Key Laboratory for Machanical Behavior of Materials，Xi'an Jiaotong University，Xi'an　710049，China）

**Abstract**：The optical transmission characteristic of colloidal photonic crystals with core @ shell structure has been calculated via the finite-difference time-domain （FDTD） method. The core @ shell structure has been designed using the low-dielectric $Fe_3O_4$ core and high-dielectric $TiO_2$ shell. The results show that the behaviors of stop band can be adjusted by the effective permittivity and core @ shell size ratio of materials. With the increase of permittivity， the stop bands show redshift and bandwidth increase. When the overall size of core @ shell is constant， the stop bands show blueshift with the increasing core diameter， and the maximum bandwidth （$\Delta\lambda/\lambda$） reaches 33. 4% when the diameter ratio between core @ shell and core is 150 nm：130 nm. When the core size is constant， the stop bands show redshift with the increase of the overall size of the core @ shell structure. The minimum thickness of $TiO_2$ shell that can make the stop bands appear is 3 nm in the $Fe_3O_4$ @ $TiO_2$ core @ shell structure.

**Key words**：photonic crystal， stop bands， optical transmission characteristic， core @ shell structure
**PACS**：42. 70. Qs，75. 40. Mg

# $Fe_3O_4$ /$TiO_2$ 核壳结构胶体光子晶体的光学传输特性分析

黄 岩，梁工英，霍 格，卢学刚*
（西安交通大学 理学院 陕西省先进功能材料及介观物理重点实验室，
金属材料强度国家重点实验室，陕西 西安　710049）

**摘要**：通过时域有限差分方法（FDTD）计算了核壳结构胶体光子晶体的光学传输特性. 这一核壳结构是由低介电的 $Fe_3O_4$ 核与高介电的 $TiO_2$ 壳构成的. 计算结果表明,阻带的行为受到材料介电常数和核壳比的调控. 随着材料介电常数的增加,阻带不断红移,并且带宽不断增大. 当核壳结构的整体尺寸一定时,随着核直径的增大,阻带不断蓝移,并且在核壳结构直径与核直径之比为 150 nm：130 nm 时,带宽最大,达到 33. 4% ;当核尺寸一定时,随着核壳结构整体尺寸的增大,阻带红移. 在 $Fe_3O_4$@ $TiO_2$ 核壳结构中,能够出现阻带的 $TiO_2$ 壳层的最小厚度是 3 nm.

**关　键　词**：光子晶体；阻带；光学传输特性；核壳结构
**中图分类号**：O433　　**文献标识码**：A

## Introduction

The concept of "Photonic Crystal" was independently suggested by Yablonovitch[1] and John[2] in 1987. When electromagnetic wave propagates in photonic crystal， due to Bragg scattering， wave of certain frequency range can be inhibited resulting in the formation of photonic band gap （PBG）. Colloidal photonic crystals are a kind of important PBG materials. They are three-dimensional periodic structures which can be obtained by self-assembly of monodisperse colloidal nanoparticles in solution， and they can shift PBGs by the periodic change of refractive index. Ge et al[3] fabricated $Fe_3O_4$ colloidal photonic crystals with magnetically tunable PBGs covering the entire visible spectrum. By changing the strength

of external magnetic field, one can obtain the effective control of PBGs[4-12]. The $Fe_3O_4$ colloidal crystals have fast optical response, reversible control, and wide tunable range[13-14]. However, it is difficult to accurately gather magnetic field in local small areas for the divergence of magnetic fields[4,15], resulting in the low tunable precision and inaccurate color effect in local small areas. Shim *et al*[16] investigated the behavior of colloidal arrays under electric field to achieve fast and precise tuning of PBGs. Colloidal photonic crystals that can be regulated by electric field for the surface charges have the advantage of accurate tunable in local small areas. While the limited charges of colloidal particles can only produce narrow tunable PBG range which greatly limits the application. To realize wider PBG, high refractive index materials, such as $TiO_2$, have attracted much attention. $TiO_2$ possesses both high refractive index and transparency in visible region which is suitable for optical photonic crystals[17-18]. Given to the combined advantage of super-paramagnetic $Fe_3O_4$ and high-dielectric $TiO_2$ that can show double response to magnetic and electric fields, we investigated the optical transmission characteristic of $Fe_3O_4@TiO_2$ core@shell colloidal photonic crystals by FDTD method in this paper. It was demonstrated that colloidal photonic crystals of low-dielectric $Fe_3O_4$ core and high-dielectric $TiO_2$ shell particles produce wider bandwidth than crystals of homogeneous particles. The effects of structural parameters on optical transmission characteristic have been discussed and the results show that there exist optimal parameters to open wide gaps. Importantly, this investigation helps greatly in design of appropriate structural parameters for the fabrication of core@shell colloidal photonic crystals, providing theoretical reference for the preparation and application of this kind of photonic crystal materials.

# 1　The theory method and structural model

FDTD method[19] directly transforms the Maxwell's equations with time variable into difference equation in Yee's grid space. In difference scheme, the electric or magnetic field component of each grid point only relates with its adjacent magnetic or electric field component and the field value of the point at last time step. The electric and magnetic field component of each point in grid space can be computed in each time step, thus the propagation of electromagnetic wave and its interaction with objects can be directly simulated with the advancement of time step. Due to the electromagnetic parameters of the simulated space in difference scheme are presented according to the spatial grid, simply setting appropriate parameters for the space point is enough.

The theory sets out from the Maxwell's equations：

$$\nabla \times E = -\mu \frac{\partial H}{\partial t} - \sigma_m H \qquad , \quad (1)$$

$$\nabla \times H = \varepsilon \frac{\partial E}{\partial t} + \sigma E \qquad , \quad (2)$$

where $\varepsilon$ and $\mu$ are the permittivity and permeability of the medium, respectively. $\sigma$ and $\sigma_m$ are the conductivity and equivalent permeability. $E$ is electric field, $H$ is magnetic field. FDTD method solves the Maxwell's equa-

tions into difference forms as follows：

$$
E_x \mid_{i,j,k}^{n+1} = \frac{\varepsilon_{i,j,k} - \sigma_{i,j,k}\frac{\Delta t}{2}}{\varepsilon_{i,j,k} + \sigma_{i,j,k}\frac{\Delta t}{2}} E_x \mid_{i,j,k}^{n} +
$$

$$
\frac{\Delta t}{\varepsilon_{i,j,k} + \sigma_{i,j,k}\frac{\Delta t}{2}}\left[ \frac{H_z \mid_{i,j,k}^{n+\frac{1}{2}} - H_z \mid_{i,j-1,k}^{n+\frac{1}{2}}}{\Delta y} - \right.
$$

$$
\left. \frac{H_y \mid_{i,j,k}^{n+\frac{1}{2}} - H_y \mid_{i,j,k-1}^{n+\frac{1}{2}}}{\Delta z} \right] \qquad , \quad (3)
$$

$$
H_x \mid_{i,j,k}^{n+1} = \frac{\mu_{i,j,k} - \sigma_m \mid_{i,j,k}\frac{\Delta t}{2}}{\mu_{i,j,k} + \sigma_m \mid_{i,j,k}\frac{\Delta t}{2}} H_x \mid_{i,j,k}^{n} -
$$

$$
\frac{\Delta t}{\mu_{i,j,k} + \sigma_m \mid_{i,j,k}\frac{\Delta t}{2}}\left[ \frac{E_z \mid_{i,j,k}^{n+\frac{1}{2}} - E_z \mid_{i,j-1,k}^{n+\frac{1}{2}}}{\Delta y} - \right.
$$

$$
\left. \frac{E_y \mid_{i,j,k}^{n+\frac{1}{2}} - E_y \mid_{i,j,k-1}^{n+\frac{1}{2}}}{\Delta z} \right] \qquad . \quad (4)
$$

The forms of $E_y$ and $E_z$ are similar with $E_x$, and the forms of $H_y$ and $H_z$ are similar with $H_x$. The periodic boundary conditions are applied[20]. Non-uniform mesh division method guarantees the precision and efficiency of the calculation process[21].

The model is square lattice of core@shell nanoparticles in air periodically arranged along $x$, $y$, $z$ directions with lattice constant $a$, as depicted in Fig. 1 and the effects of electromagnetic loss during the transmission are ignored since the high frequency in the visible area. The permittivity and diameters of core and shell are $\varepsilon_1$, $\varepsilon_2$ and $D_{core}$, $D_{core-shell}$, respectively. The period is $N$.
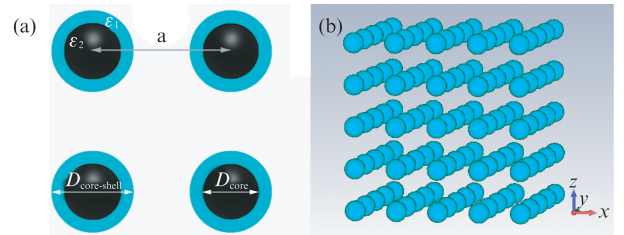


Fig. 1　3D square lattice of core@shell photonic crystal（a）square lattice and structure parameters, and（b）periodic array from above nanospheres
图 1　三维正方核壳结构光子晶体（a）正方晶格及结构参数，（b）纳米球的周期性排列

# 2　Numerical simulation results and discussion

## 2.1　The influence of permittivity $\varepsilon$ on the optical transmission characteristic

The homogeneous dielectric spheres periodically arrange with $a = 300$ nm and diameter of spheres $d = 150$ nm, $N = 5 \times 10 \times 5$. In the situation of normal incidence, the light propagates along $y$ direction. The FDTD simulation results in Fig. 2 clearly suggest that the higher permittivity $\varepsilon$ produces a wider bandwidth and that the
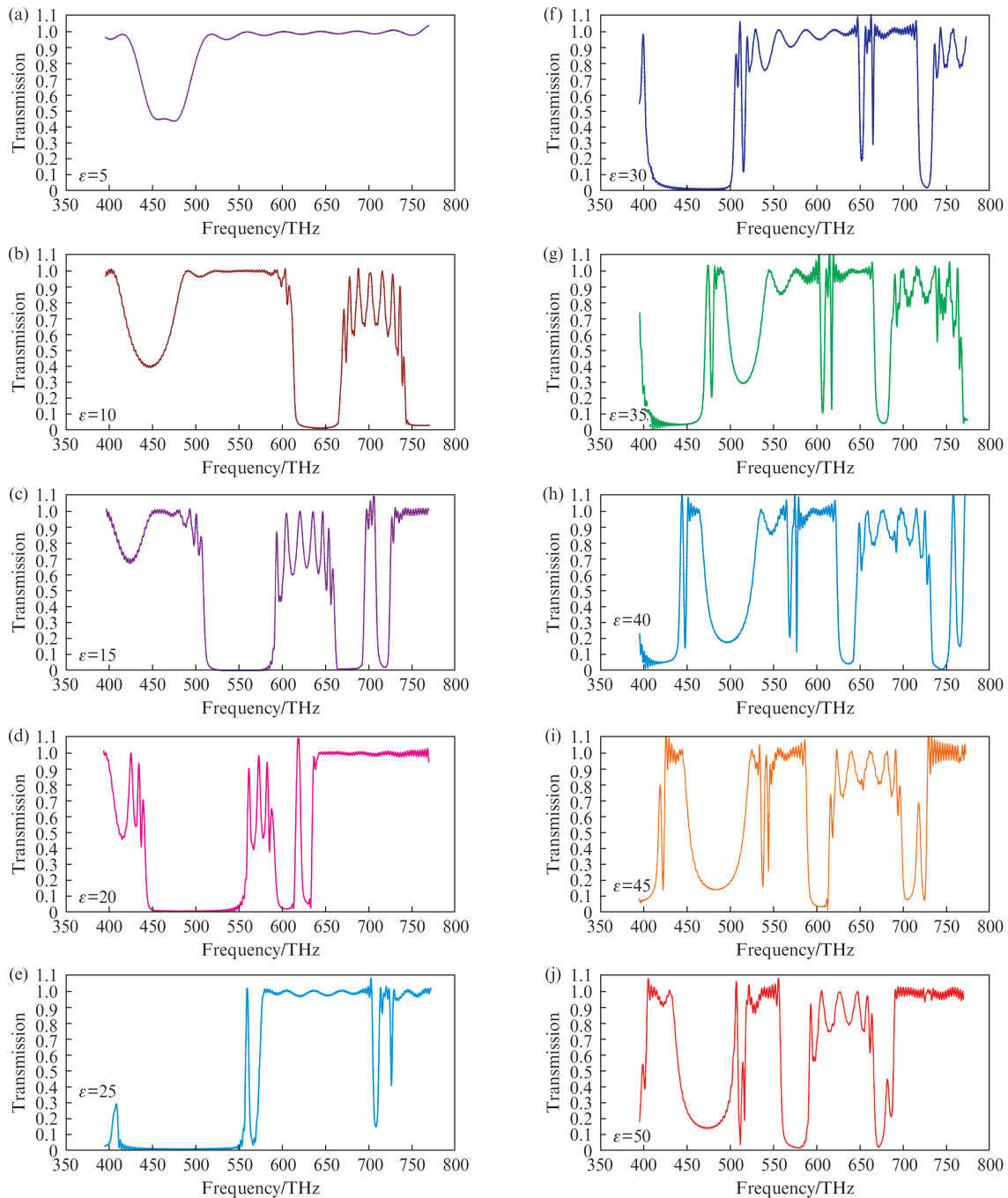
Fig. 2 The optical transmission spectra of photonic crystals with the same lattice constant (300 nm), diameter (150 nm) and different permittivities

图 2 相同晶格常量(300 nm)、颗粒直径(150 nm),不同介电常数下的光子晶体光学传输谱

position of stop bands continuously moves to longer wavelength with $\varepsilon$ from 5 to 50. In addition, the bandwidth tends to decrease upon the PBG closing to infrared region.

When the permittivity of the sphere is small ($\varepsilon = 5$), the permittivity contrast between dielectric sphere and background is too small to produce obvious stop bands. As $\varepsilon = 10$, the obvious stop band appears in 453 ~ 484 nm. Then it shows redshift and increasing bandwidth as $\varepsilon$ ranging from 10 to 25; the maximum bandwidths ($\Delta\lambda/\lambda$) are 27% as $\varepsilon$ reaches to 25. The

stop band continues to red shift but with decreasing bandwidth for $\varepsilon$ from 30 to 40. At the same time, the new stop band appears when $\varepsilon = 30$ and shows the same changing tendency with the increase of permittivity as above.

## 2.2 The influence of $Fe_3O_4$@$TiO_2$ core@shell ratio on the optical transmission characteristic

In this part, we discuss the influence on the optical transmission characteristic exerted by core@shell ratio. At first, the permittivity of $Fe_3O_4$ and $TiO_2$ (anatase for actual simulation) is 9 and 48.

## 2. 2. 1　Adjusting the size of $Fe_3O_4$-core with the fixed overall size of the core@shell structure

The model is $Fe_3O_4$ @ $TiO_2$ core @ shell structure with $a = 300$ nm, $N = 5 \times 10 \times 5$, $D_{core-shell} = 150$ nm, and $D_{core}$ varies from 0 to 150 nm, and the increment is 10 nm. In this process, the structure gradually transforms from pure $TiO_2$ nanosphere to $Fe_3O_4$@ $TiO_2$ core@ shell structure and to pure $Fe_3O_4$ nanosphere at last, such as those depicted in Fig. 3.

When the structure is pure $TiO_2$ nanosphere which means the diameter of $Fe_3O_4$-core $D_{core} = 0$ nm, the stop band appears in 504 ~ 516 nm. It keeps stable in 503 ~ 516 nm and the bandwidth is 2.4% with the $D_{core}$ increasing from 0 nm to 30 nm. It gradually moves to shorter wavelength (blueshift) until it shifts out of the visible region and into the near ultraviolet region in
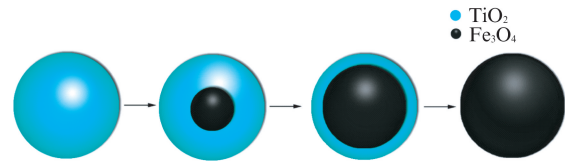


Fig. 3　The structural transformation with the increasing $D_{core}$
图 3　核直径 $D_{core}$ 增长引起的结构转变

$D_{core} = 90$ nm. Meanwhile, the new stop band appears with blueshift just the same as before and the bandwidth reaches maximum 33.4% as $D_{core} = 130$ nm. At last, the structure transforms into pure $Fe_3O_4$ nanosphere and shows the stop band in 435 ~ 465 nm with the bandwidth reaching to 6.7% as $D_{core} = 150$ nm, just as Fig. 4.
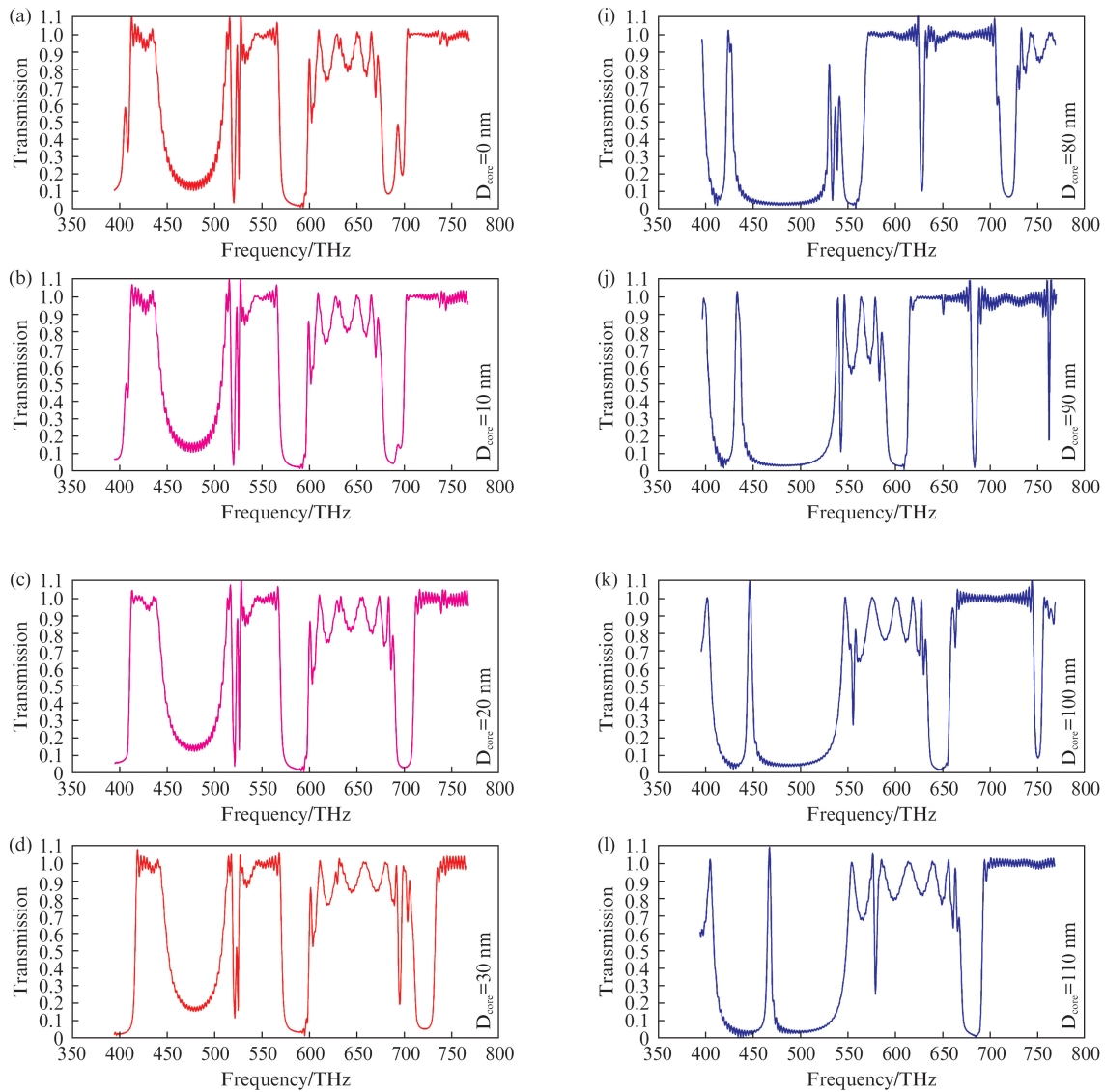
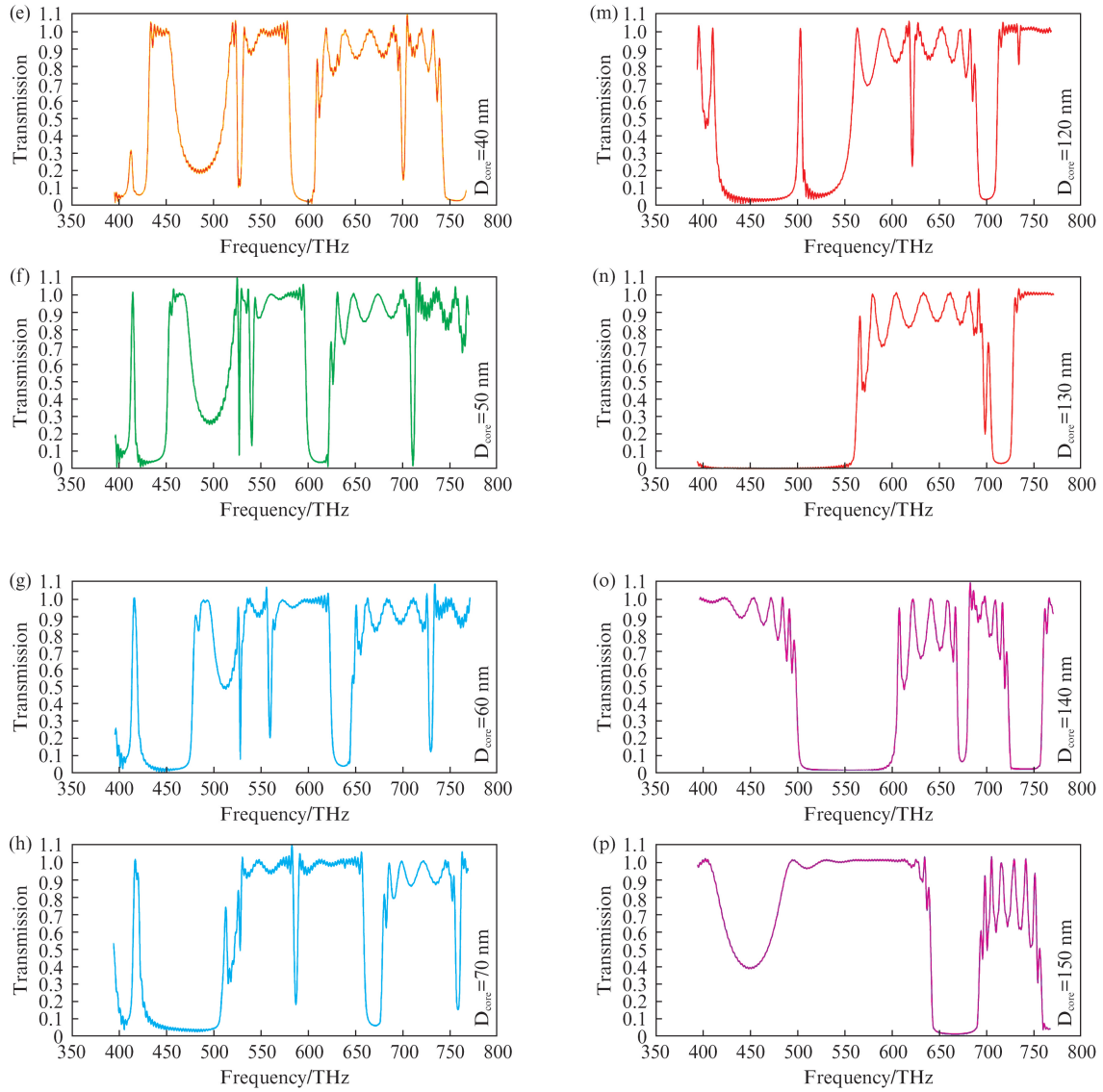Fig. 4    The optical transmission spectra of different core@ shell ratios with $D_{core\text{-}shell}$ = 150 nm and varying $D_{core}$ ( 0 ~ 150 nm )

图 4    不同核壳比( $D_{core\text{-}shell}$ = 150 nm , $D_{core}$ 由 0 到 150 nm )下的光子晶体光学传输谱

Altogether, fixing the overall size of core @ shell structure, PBGs gradually blueshift with the increasing size of $Fe_3O_4$-core and the bandwidth reaches maximum as $D_{core\text{-}shell}$ : $D_{core}$ = 150 nm: 130 nm. The effective refractive index of core@ shell structures can be computed from Eq. 5[14] :

$$n_{eff} = \frac{R_{core}^3}{R_{core\text{-}shell}^3} n_{core} + \left( 1 - \frac{R_{core}^3}{R_{core\text{-}shell}^3} \right) n_{shell}    . (5)$$

In the situation that the overall size of the core @ shell structure $R_{core\text{-}shell}$ is fixed and the size of $Fe_3O_4$ nanosphere $R_{core}$ is increased, Eq. 5 can be simplified as

$$n_{eff} = k_1 - k_2 R_{core}^3        ,    (6)$$

$k_1$ , $k_2$ are constants. It is obvious that the effective refractive index of core@ shell decreases with the increase of $R_{core}$. According to the relation between permittivity and refractive index of the medium ( $n = \sqrt{\mu\varepsilon}$ ), at this time, the permittivity of core @ shell structure also decreases resulting in the blueshift of PBGs. In addition, analyzing the Eq. 6, $n_{eff} \propto - R_{core}^3$, when the value of $R_{core}$ is small ( 0 ~ 15 nm ), the contrast of $n_{eff}$ for each $R_{core}$ is also small, which produced the similar stop bands as depicted in Fig. 4 for $D_{core}$ = 0 ~ 30 nm. When $R_{core} \geqslant$ 60 nm, the contrast of $n_{eff}$ for each $R_{core}$ increased sharply, resulting in the obvious differences of stop bands just as Fig. 4 for $D_{core}$ = 120 ~ 150 nm.

Furthermore, our previous works showed that for the pure $Fe_3O_4$ nanosphere arrays with $a$ = 300 nm, only when the particle size reached the critical value ( $D_{Fe_3O_4}$ = 130 nm ) can we observe the obvious PBGs. What's more, the PBGs showed redshift with increasing $D_{Fe_3O_4}$ while the research in this paper shows a new result that when the overall size of core @ shell structure is fixed, the PBG will show blueshift with increasing $D_{Fe_3O_4}$ and no

matter how small the $D_{Fe_3O_4}$ is, the PBG can be available which means there's no critical value of $D_{Fe_3O_4}$ in this situation. We believe that the existence of $TiO_2$-shell plays an important role in the occurrence of PBGs. Thus, coating high refractive index materials ($TiO_2$) on the surface of low refractive index materials ($Fe_3O_4$) is very significant for the appearance of PBGs.

## 2.2.2  Adjusting the overall size of the core@ shell structure with the fixed size of $Fe_3O_4$-core

The model in this part is $Fe_3O_4$@ $TiO_2$ core@ shell structure with $a = 300$ nm, $N = 5 \times 10 \times 5$, $D_{core} = 100$ nm, and $D_{core\text{-}shell}$ ranges from 102 nm to 130 nm. Fig. 5 shows that there are no PBGs when $D_{core\text{-}shell}$ is

102 ~ 104 nm, then PBGs appeared as 412 ~ 422 nm for $D_{core\text{-}shell} = 106$ nm, 440 ~ 452 nm for $D_{core\text{-}shell} = 108$ nm, and 462 ~ 483 nm for $D_{core\text{-}shell} = 110$ nm. The bandwidths are 2.4%, 2.7% and 4.4%, respectively. 551 ~ 613 nm for $D_{core\text{-}shell} = 120$ nm, 588 ~ 652 nm for $D_{core\text{-}shell} = 130$ nm and 577 ~ 682 nm for $D_{core\text{-}shell} = 160$ nm. As a result, PBGs show obvious redshift with increasing $D_{core\text{-}shell}$, and the photonic crystal inclines to scatter shorter wavelength for smaller $D_{core\text{-}shell}$, while PBGs incline to appear in longer wavelength for the bigger one. The minimum thickness of $TiO_2$-shell is 3 nm and with the increasing shell's thickness, the bandwidth increases and PBGs shift to longer wavelength.
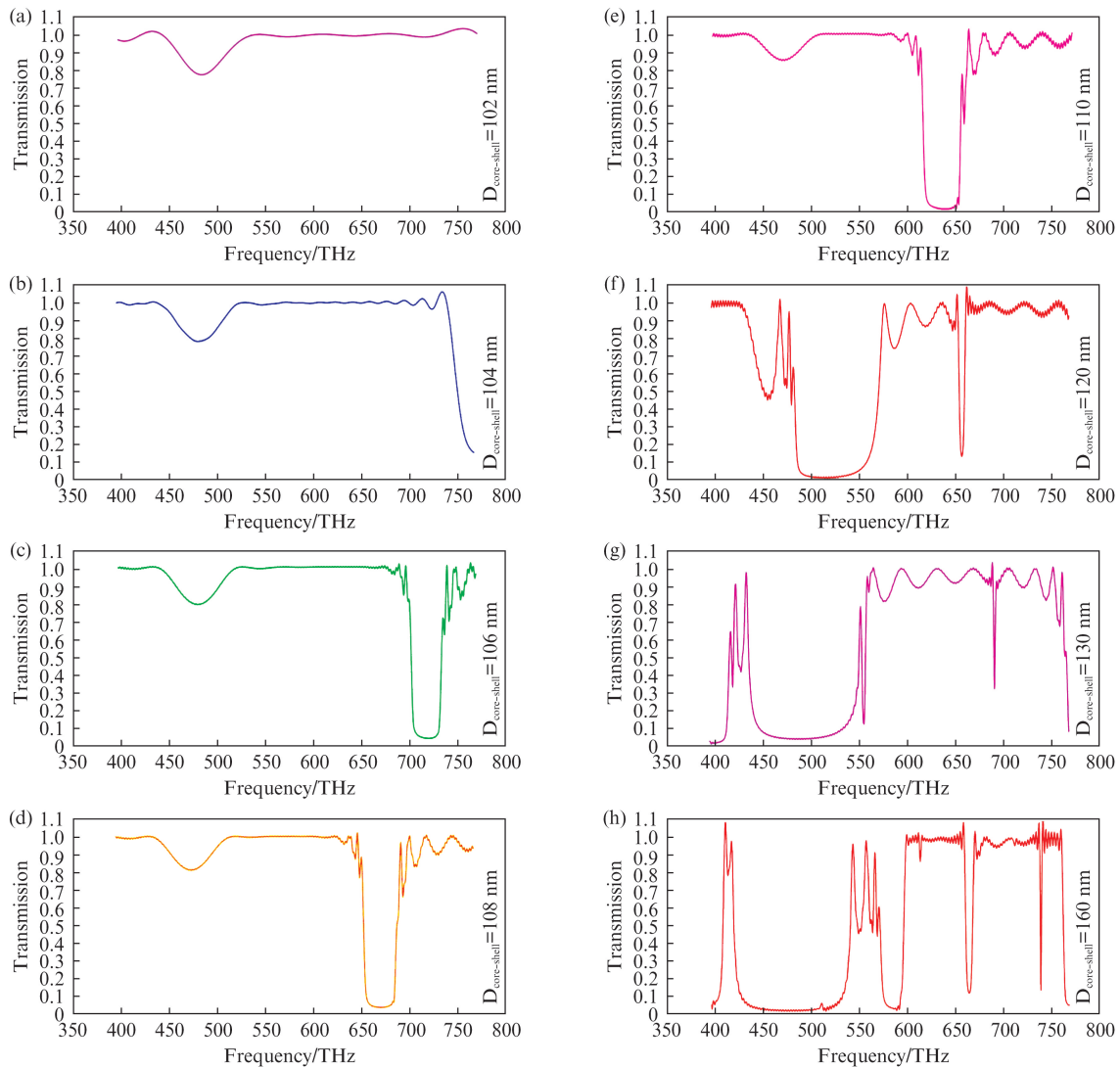


Fig. 5  The optical transmission spectra of different core@ shell ratios with $D_{core} = 100$ nm and varying $D_{core\text{-}shell}$ (102 ~ 160 nm)

图 5  不同核壳比($D_{core} = 100$ nm，$D_{core\text{-}shell}$由 102 到 160 nm)下的光子晶体光学传输谱

What's more, in the situation that adjusts the overall size of core-shell structure with fixed size of $Fe_3O_4$-core, Eq. 5 can be simplified as

$$n_{eff} = k_3 - \frac{k_4}{R_{core\text{-}shell}^3} \quad , \quad (7)$$

$k_3$, $k_4$ are constants. It is obvious that the effective refractive index of core@ shell increases with the increase of $R_{core\text{-}shell}$, resulting in the redshift of PBGs. Because of $n_{eff} \propto -\dfrac{1}{R_{core\text{-}shell}^3}$, the influence of $n_{eff}$ with each $R_{core\text{-}shell}$ is

obvious when $R_{\text{core-shell}}$ is small ( $D_{\text{core-shell}}$ = 102 ～ 110 nm), which produces obvious redshift for PBGs in Fig. 5. However, with the increase of $D_{\text{core-shell}}$ from 120 to 160 nm, the change of $n_{\text{eff}}$ lowers resulting in the decreasing redshift of PBGs in contrast with small $D_{\text{core-shell}}$.

## 3   Conclusions

$Fe_3O_4 @ TiO_2$ core @ shell nanoparticles can show double response to magnetic and electric fields. This kind of colloidal photonic crystal has importantly practical significance. In this paper, we study the optical transmission characteristic of photonic crystals with core @ shell structure via FDTD method. The non-uniform mesh division method guarantees the precision and efficiency of the calculation process. Hence, we offered detailed analysis of the optical transmission characteristic of $Fe_3O_4 @ TiO_2$ core@ shell colloidal photonic crystals from the aspect of structural parameters, including permittivity and core@ shell ratio. The PBGs show obvious redshift and increasing bandwidth with the increasing particles' permittivity. The core@ shell ratio from two aspects was discussed, adjusting the size of $Fe_3O_4$-core with the fixed overall size of the core@ shell structure and adjusting the overall size of the core@ shell structure with the fixed size of $Fe_3O_4$-core. The PBGs show blueshift for the former while redshift for the latter with the increase of the variables. The minimum thickness of $TiO_2$ shell that can make PBGs appear was 3 nm in $Fe_3O_4 @ TiO_2$ core @ shell structure. These results provide theoretical reference for the preparation and application of core@ shell colloidal photonic crystal materials.

## References

[1] Yablonovitch E. Inhibited spontaneous emission in solid-state physics and electronics[J]. *Phys. Rev. Lett.* 1987, **58**(20): 2059 − 2062.

[2] John S. Strong localization of photons in certain disordered dielectric superlattices[J]. *Phys. Rev. Lett.* 1987, **58**(23): 2486 − 2489.

[3] Ge J P, Hu Y X, Yin Y D. Highly tunable superparamagnetic colloidal photonic crystals[J]. *Angew. Chem.* 2007, **119**(39): 7572 − 7575.

[4] Ge J P, Yin Y D. Magnetically responsive colloidal photonic crystals [J]. *J. Mater. Chem.* 2008, **18**(42): 5041 − 5045.

[5] He L, Wang M S, Zhang Q, *et al*. Magnetic assembly and patterning of general nanoscale materials through nonmagnetic templates [J]. *Nano Lett.* 2012, **13**(1): 264 − 271.

[6] He L, Hu Y X, Han X G, *et al*. Assembly and photonic properties of superparamagnetic colloids in complex magnetic fields[J]. *Langmuir.* 2011, **27**(22): 13444 − 13450.

[7] He L, Wang M S, Ge J P, *et al*. Magnetic assembly route to colloidal responsive photonic nanostructures[J]. *Accounts Chem. Res.* 2012, **45** (9): 1431 − 1440.

[8] He L, Hu Y X, Kim H, *et al*. Magnetic assembly of nonmagnetic particles into photonic crystal structures[J]. *Nano Lett.* 2010, **10**(11): 4708 − 4714.

[9] Ge J P, Kwon S, Yin Y D. Niche applications of magnetically responsive photonic structures[J]. *J. Mater. Chem.* 2010, **20**(28): 5777 − 5784.

[10] Yang Y, Gao L, Lopez G P, *et al*. Tunable assembly of colloidal crystal alloys using magnetic nanoparticle fluids[J]. *ACS nano.* 2013, **7** (3): 2705 − 2716.

[11] Zhang Q, Janner M, He L, *et al*. Photonic labyrinths: two-dimensional dynamic magnetic assembly and in situ solidification [J]. *Nano Lett.* 2013, **13**(4): 1770 − 1775.

[12] Lin M H, Huang H L, Liu Z T, *et al*. Growth-dissolution-regrowth transitions of $Fe_3O_4$ nanoparticles as building blocks for 3D magnetic nanoparticle clusters under hydrothermal conditions [J]. *Langmuir.* 2013, **29**(49): 15433 − 15441.

[13] Ge J P, Yin Y D. Responsive photonic crystals[J]. *Angewandte Chemie International Edition.* 2011, **50**(7): 1492 − 1522.

[14] Ge J P, Hu Y X, Zhang T R, *et al*. Self-assembly and field-responsive optical diffractions of superparamagnetic colloids[J]. *Langmuir.* 2008, **24**(7): 3671 − 3680.

[15] Xu X L, Majetich S A, Asher S A. Mesoscopic monodisperse ferromagnetic colloids enable magnetically controlled photonic crystals[J]. *J. Am. Chem. Soc.* 2002, **124**(46): 13864 − 13868.

[16] Shim T S, Kim S H, Sim J Y, *et al*. Dynamic modulation of photonic bandgaps in crystalline colloidal arrays under electric field[J]. *Adv. Mater.* 2010, **22**(40): 4494 − 4498.

[17] Han M G, Shin C G, Jeon S J, *et al*. Full color tunable photonic crystal from crystalline colloidal arrays with an engineered photonic stopband[J]. *Adv. Mater.* 2012, **24**(48): 6438 − 6444.

[18] Liu D X, Yates M Z. Fabrication of size-tunable $TiO_2$ tubes using rod-shaped calcite templates [J]. *Langmuir.* 2007, **23**(20): 10333 − 10341.

[19] Yee K S. Numerical solution of initial boundary value problems involving Maxwell's equations[J]. *IEEE Trans. Antennas Propag.* 1966, **14**(3): 302 − 307.

[20] Ge D B, Yan Y B. *Finite-difference time-domain method for electromagnetic waves* [M]. Second ed. Xi'an: Press of Xidian University, 2005: 45 − 113.

[21] Wang W D, Wang J X, Li Y, *et al*. Convolutional perfectly matched layer absorbing boundary condition of the finite-difference time-domain method for the microstrip antenna[C]. *In Computing, Measurement, Control and Sensor Network (CMCSN), 2012 International Conference on IEEE*, 2012: 125 − 128.